Supplemental information

An on-chip Cell-SELEX process for automatic selection of high-affinity aptamers specific to different histologically-classified ovarian cancer cells

Lien-Yu Hung[a], Chih-Hung Wang[a], Keng-Fu Hsu[b], Cheng-Yang Chou[b] and Gwo-Bin Lee[a, c, d*]

[a]Department of Power Mechanical Engineering, National Tsing Hua University, Hsinchu, Taiwan 30

[b]Department of Obstetrics and Gynecology, National Cheng Kung University, Tainan, Taiwan 701

[c]Institute of Biomedical Engineering, National Tsing Hua University, Hsinchu, Taiwan 300

[d]Institute of NanoEngineering and Microsystems, National Tsing Hua University, Hsinchu, Taiwan 300

I. The experimental protocol of the on-chip Cell-SELEX

Supplemental Table 1 Detailed information about the experimental protocol on the Cell-SELEX microfluidic platform

Step	Procedure	Sample volume (μL)	On-chip operation condition
1.	Load ssDNA library (1 μM) into the ssDNA chamber	40	Turn on heating area at 95℃ for 5 min and then turn it off
	Load the target cell-bound magnetic beads (10^5/20 μL) into the chambers of target cell region (four open-chamber micromixers/micropumps)	20	Turn on the cooling area to keep the reagents fresh
	Load the control cell-bound magnetic beads (10^5/20 μL) into the chambers of control cell region (four open-chamber micromixers/micropumps)	20	
	Load the binding buffer into the binding buffer chamber	200	
	Load the washing buffer into the wash buffer chamber	400	
	Load the PCR reagent into the PCR chambers	23	
2.	Transport 5 μL ssDNA library into the chambers of target cell region and incubate with the target cells for 15 min		-40 kPa and 1 Hz for the open-chamber micromixer/micropump
3.	Use a magnet to collect the cell-bound magnetic beads onto the surface of incubation chamber for 1 min		
4.	Remove the supernatant through the waste chamber		-80 kPa for the vacuum pressure
5.	Transport the washing buffer into the the chambers of target cell region	40	
6.	Wash the collected cell-bound magnetic beads using the open-chamber micromixer/micropump for 1 min		Various vacuum pressures (form -40 to -80 kPa) and 1 Hz for the open-chamber micromixer/micropump
7.	Repeat the steps 3–5 for six times		
8.	Transport the binding buffer to re-suspend the cell-bound magnetic beads in the chambers of target cell region	20	
9.	Thermal lysis of the target cells and attached ssDNA		Turn on heating area at 95℃ for 10 min and then turn it off
10.	Transport the bound ssDNA into the chambers of control cell region for negative selection	10	-80 kPa and 20 Hz for the S-shape micropump
11.	Incubate the bound ssDNA with the control cells for 15 min		-40 kPa and 1 Hz for the open-chamber micromixer/micropump
12.	Use a magnet to collect the control cell-bound magnetic beads onto the surface of incubation chamber for 5 min		
13.	Transport supernatant to the PCR chamber for amplification of the screened sequence	2	-80 kPa and 1 Hz for the open-chamber micromixer/micropump
14.	Finally, take 5 μL of PCR product for the next round		

II. Competitive testing of aptamer candidates from randomly selected TA colonies

A competitive test using label-free target cells as competitors for aptamers against target cells coated with Epithelial Enriched beads was performed, as illustrated in Supplemental Figure 1. The “negative test” condition was with the Epithelial Enriched beads incubated alone (i.e. without target cells) with the aptamer

candidates. Because few aptamer candidates would bind to the Epithelial Enriched beads, it was expected that only a very weak or no PCR signal would be observed for this case, after PCR amplification. The "competitive testing" process was then performed with the label-free target cells and target cell-magnetic bead complexes were incubated together with the aptamer candidates. Free target cells would bind with some of the aptamer candidates, but they could not be collected by using a magnet. Therefore, it was expected that weak PCR signals would be observed for this case after PCR amplification. The "positive test" condition was when only target cell-magnetic bead complexes were incubated with the aptamer candidates. Therefore, it was expected that strong PCR signals would be observed for this case after PCR amplification.

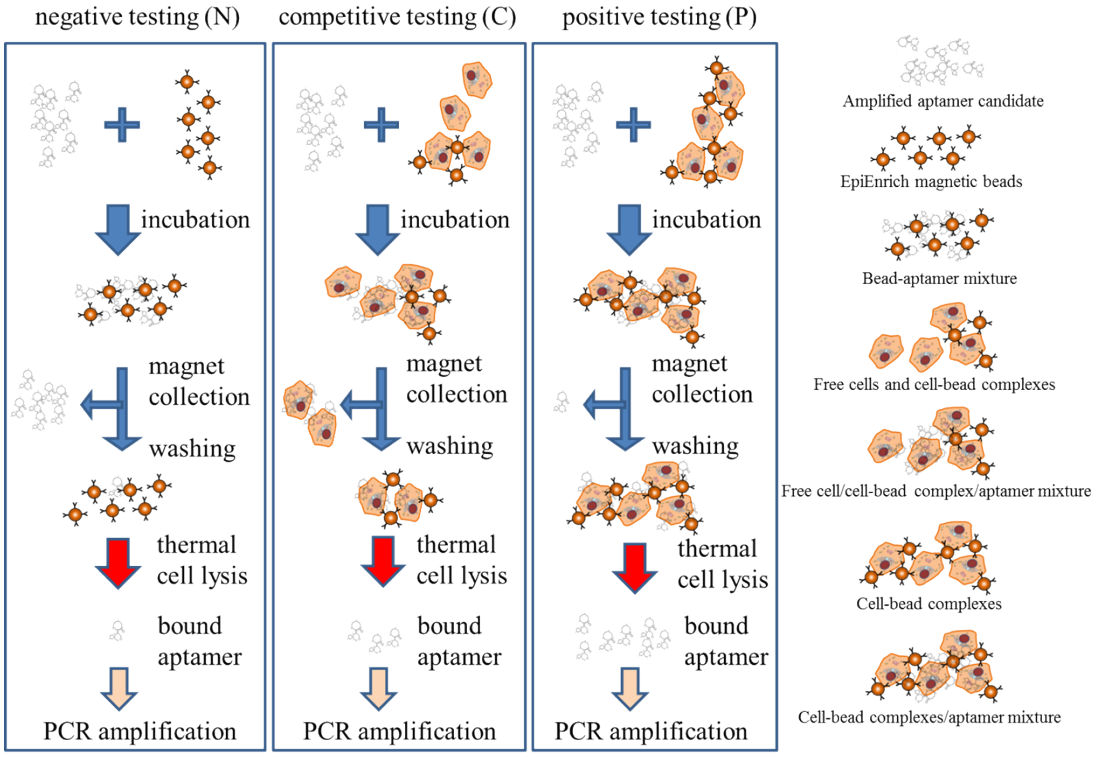

Supplemental Figure 1. Illustrations of the positive, competitive, and negative assays.

III. Illustration of MyOne bead coating with aptamer and EpiEnrich beads application

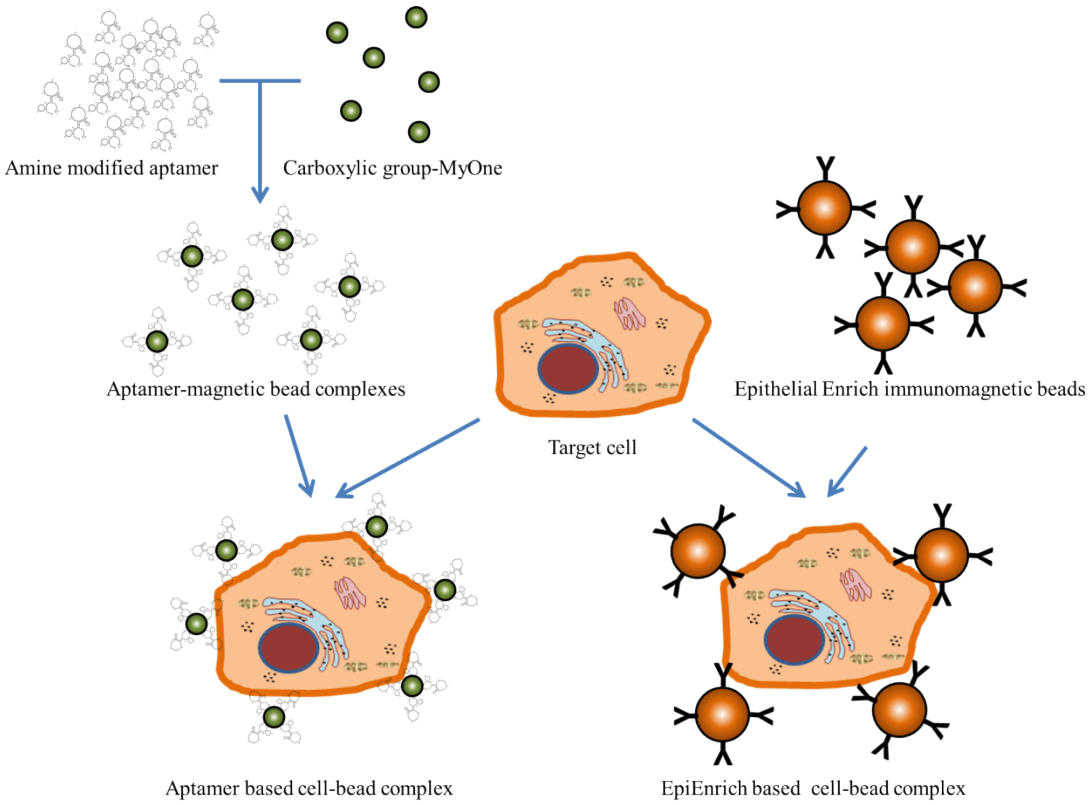

Supplemental Figure 2. Illustrations of Epithelial Enrich immunomagnetic beads application and MyOne magnetic beads coating

IV. Measurements of integrated microfluidic chip, the flow pumping rate and the mixing index

The integrated microfluidic chip was consisted of three layers, including two

layers of PDMS and one glass substrate. The first PDMS layer was a thin layer with a thickness of 100 μm, which was a liquid channel layer. Another thick PDMS layer (around 800 μm), which contained air channels, was used to control this integrated microfluidic system.

The main function of the transportation unit of the microfluidic chip was to transport the binding buffer and the washing buffer to the target cell region. Because the transport process requires three steps, reducing the operating time for each fluid transport step would effectively increase the overall flow rate. The fluidic pumping rate was also found to increase with an increase in the applied gauge pressure (i.e. higher vacuum), as shown in Supplemental Figure 2(A). The maximum pumping rate of the transportation unit was found to be 941.2 μL/min when operated at a frequency of 0.67 Hz at a gauge pressure of -80 kPa.

Similarly, the S-shape micropumps were used to transport the thermally-released ssDNA into the control cell region. However, the S-shape micropumps were operated at a higher driving frequency so that the fluid was more efficiently transported. Furthermore, the 3-cm-long microchannel between the heating and the cooling areas contained 7 μL of fluidic dead volume so these S-shape micropumps could not transport sufficient reagents under a lower driving frequency. The maximum pumping rate of the S-shape micropump was experimentally found to be

29.3 μL/min when driven at a frequency of 20.0 Hz at a gauge pressure of -80 kPa, as shown in Supplemental Figure 2(B).

The open-chamber micropumps of the control cell region were used to transfer the unbound ssDNA supernatant to the PCR chambers. The pumping rate of the open-chamber micropump was measured to be 242.1 μL/min when operated at a frequency of 4.0 Hz at a gauge pressure of -80 kPa, as shown in Supplemental Figure 2(C).

The mixing efficiency of the open-chamber micromixer was also explored. A fixed volume of red ink was first loaded in the micromixer and images of the mixing process were then captured by a high-speed charge-coupled device (CCD) camera (MC1311, Mikrotron, Germany), in conjunction with a high-speed image acquisition interface card (INSPECTA-5, Mikrotron, Germany) under a fluorescence microscope (E-400, Nikon, Japan). The recorded images were then analyzed by using digital image processing techniques to determine the mixing index which is used to characterize the mixing performance. The mixing index (σ) is defined as follows.

$$\sigma(A) = \left(1 - \frac{\int_A \left|C^+ - C_\infty^+\right| dA}{\int_A \left|C_0^+ - C_\infty^+\right| dA}\right) \times 100\%,$$

(1)

which σ(A) is the mixing index for the normalized concentration (C^+) distributing in

the cross-section of the mixing chamber (A). C_0^+ is the normalized initial condition, and C_∞^+ is the completely mixed condition with normalization ($C_\infty^+ = 0.5$). $\sigma = 0\%$ means that the sample is completely unmixed. When the sample is completely mixed, the σ is 100%, as shown in Supplemental Figures 2(D) and (E).

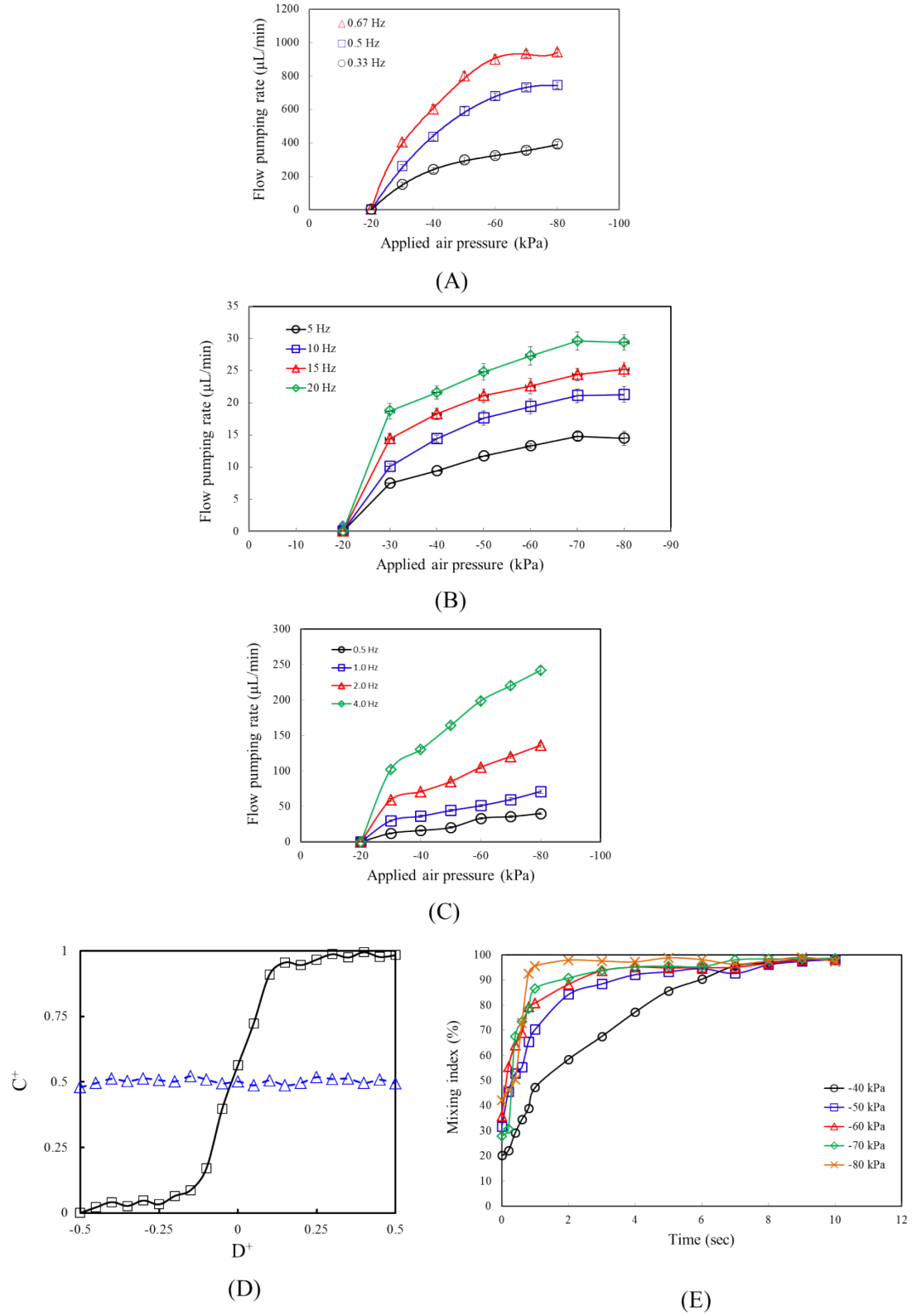

Supplemental Figure 3. Characterization of the micropumps and micromixers for Cell-SELEX of OvCa. (A) The relationship between the pumping rate and the applied

gauge pressure for the transportation unit when operated at different driving frequencies. The maximum pumping rate of the transportation unit was experimentally found to be 941.2 μL/min when operated at 0.67 Hz and -80 kPa; (B) The relationship between the pumping rate and the applied gauge pressure for the S-shape micropump when operated at different driving frequencies. The maximum pumping rate was measured to be 29.3 μL/min at 20.0 Hz and -80 kPa; (C) The relationship between the pumping rate and the applied gauge pressure for the open-chamber micropump located at the control cell region when operated at different driving frequencies. The maximum pumping rate was measured to be 242.1 μL/min at 4.0 Hz and -80 kPa; (D) Normalized concentrations along the center of the open-chamber micromixer/micropump; (E) The relationship between the mixing time and mixing index when operated at different gauge pressures. The mixing index increased from 42.1% to 95.5% when the driving conditions were set to -80 kPa, 1.0 Hz, and 1 second.

V. The ssDNA-folding structure of the selected aptamers

Supplemental Figure 4 shows the predicted ssDNA-folding structures of the aptamers at 25℃, using MFOLD software version 3.5 (available at http://mfold.rna.albany.edu/)

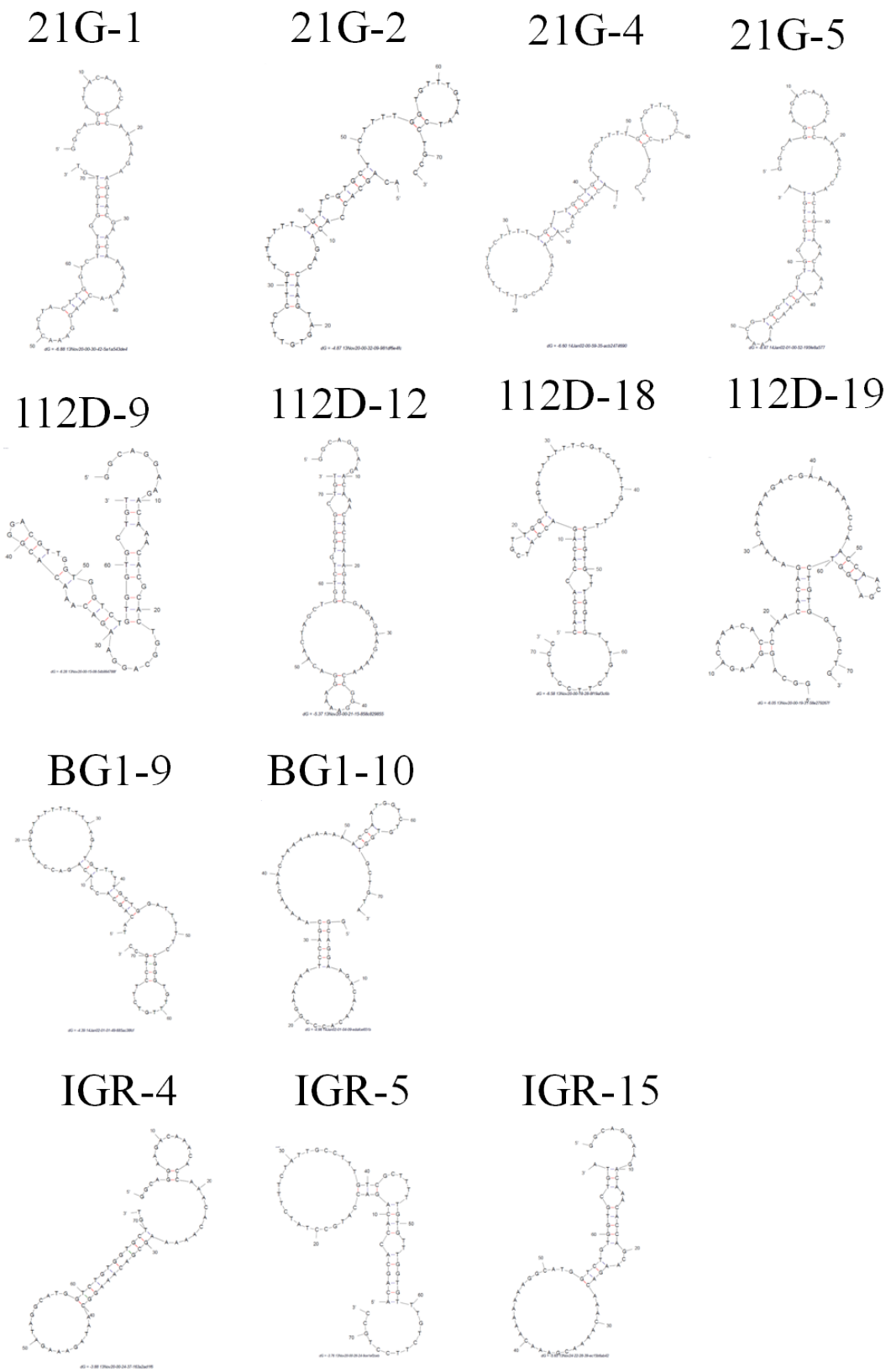

Supplemental Figure 4: The ssDNA-folding structures of four TOV21G-specific aptamers, including 21G-1, 21G-2, 21G-4 and 21G-5; four TOV112D-specific

aptamers, including 112D-9, 112D-12, 112D-18 and 112D-19; two BG-1-specific aptamers, including BG1-9 and BG1-10; three IGROV1-specific aptamers, including IGR-4, IGR-5 and IGR-15.

VI. Cell capture rates after using manual washing steps

Cells were incubated with specific aptamer-coated magnetic beads by using a larger-scale shaker (INTELLI-MIXER, ELMI Ltd, Latvia) for 30 minutes. After a manual washing process using a sampler micro-pipette (Pipetman, RAININ, Anachem Ltd., United Kingdom), the magnetic-bead complexes conjugated to cells were subjected to hemocytometer analysis under a microscope. The measured cell capture rates for four different cell lines are listed in Supplemental Table 1.

Supplemental Table 2: Cell capture rates after manual washing steps

Cell line[a] / Aptamer	TOV21G	TOV112D	BG1	IGROV1
EpiEnrich[b]	91.2	88.0	98.4	99.0
21G-1	87.7	93.7	68.0	95.7
21G-2	87.8	95.0	95.8	98.8
21G-4	90.1	91.9	79.3	93.2
21G-5	86.8	89.7	88.1	95.7
112D-9	88.1	91.7	93.7	99.1
112D-12	99.5	98.1	96.9	99.5
112D-18	96.4	96.8	92.9	98.5
112D-19	87.3	93.9	92.9	98.7
BG1-9	94.1	91.9	95.2	94.5
BG1-10	89.0	88.9	98.1	95.6
IGR-4	94.8	91.8	86.8	98.6
IGR-5	94.8	96.2	83.0	98.4
IGR-15	81.9	88.1	90.4	87.3

VII. Cell capture rates after using on-chip washing

In addition to the manual washing process, on-chip washing using the open-chamber micromixers/micropumps was also tested for the resulting cell capture rates. The results are listed in Supplemental Table 2. Four TOV21G-specific aptamers, including 21G-1, 21G-2, 21G-4 and 21G-5, showed relatively high capture rates toward TOV21G (target cells) (68.9±2.9%, 76.6±8.4, 81.8±1.3% and 79.8±7.6%,

respectively). However, 21G-1, 21G-4 and 21G-5 aptamers could also capture IGROV1 (non-target cells) with capture rates of 39.9±4.8%, 47.1±3.5% and 36.2±9.7%, respectively, which may lead to non-specific binding issues if used for OvCa diagnosis. Furthermore, 21G-2 and 21G-5 aptamers also captured M2-B104 (non-target cells) with capture rates of 38.6±4.1% and 43.7±3.5%, respectively. Note that the capture rates for all other cell lines were lower than 40%, indicating that these four TOV21G-specific aptamers can capture more TOV21G cells than other cancer cell lines. All statistical analysis is shown in the Supplemental Information Table S2.

Similarly, four TOV112D-specific aptamers, including 112D-9, 112D-12, 112D-18 and 112D-19, showed relatively high capture rates toward TOV112D (target cells; 58.8±8.3%, 61.6±1.6, 62.5±10.3% and 52.9±10.7%, respectively). However, all of them also captured TOV21G (non-target cells) with capture rates of 39.9±11.6%, 40.7±8.4%, 38.1±2.7% and 41.4±9.5%, respectively, which may cause non-specific binding issues for further OvCa diagnosis, even though all of these capture rates showed significant statistical variation. Furthermore, 21G-2 and 21G-5 aptamers captured M2-B104 (non-target cells) with capture rates of 38.6±4.1% and 43.7±3.5%, respectively. It is important to note that the capture rates for all the other cell lines were lower than 40%, indicating that these four TOV112D-specific aptamers can capture more TOV112D cells than the other cancer cell lines. All statistical analysis is

shown in the Supplemental Information Table S2.

Similarly, two BG-1-specific aptamers, including BG1-9 and BG1-10, showed relatively high capture rates toward BG-1 (target cells; 74.5±14.0% and 72.8±15.4%, respectively), indicating that these two BG-1-specific aptamers can capture more BG-1 cells than other cancer cell lines. All statistical analysis results are shown in the Supplemental Information Table S2.

Furthermore, three IGROV1-specific aptamers, including IGR-4 and IGR-5, showed relatively high capture rates toward IGROV1 (target cells) (53.0±6.9% and 51.8±3.8%, respectively). However, the IGR-15 aptamer only showed a cell capture rate of 27.1±4.3% toward IGROV1. It is important to note that only IGR-4 and IGR-5 can capture more IGROV1 cells than other cancer cell lines. The complete statistical analysis are shown in the Supplemental Information Table S2

Supplemental Table 3: Cell capture rates after on-chip washing

Cell line[a]	TOV21G	TOV112D	BG1	IGROV1	HeLa	MCF7	A549	HepG2	M2-B104	NIH3T3
EpiEnrich[b]	14.5±3.2	3.5±1.9	32.7±2.4	38.2±13.7	35.8±4.7	83.1±4.1	68.6±5.4	3.5±1.2	8.9±3.1	14.2±4.4
MyOne	1.1±0.2	0.4±0.1	1.5±0.4	3.8±1.2	0.9±0.1	0.3±0.1	1.1±0.4	1.4±0.2	2.9±0.9	3.5±1.1
21G-1	68.9±2.9	23.7±9.0	15.1±4.7	39.9±4.8	23.6±3.5	14.1±5.3	17.9±2.2	22.4±7.0	31.0±6.8	20.9±7.1
21G-2	76.6±8.4	20.2±8.1	28.0±10.8	30.2±10.7	9.6±1.3	32.5±12.1	21.9±3.1	34.3±6.4	38.6±4.1	24.7±6.9
21G-4	81.8±1.3	27.7±10.3	15.0±7.5	47.1±3.5	15.0±1.1	24.3±4.8	24.7±4.5	17.1±4.0	14.1±3.3	17.1±1.4
21G-5	79.8±7.6	24.1±9.1	21.5±6.3	36.2±9.7	12.5±2.1	21.4±3.9	15.7±0.9	24.2±3.3	43.7±3.5	30.4±6.3
112D-9	39.9±11.6	58.8±8.3	28.3±9.5	30.1±5.5	23.0±1.9	29.1±2.9	34.1±0.8	18.9±5.1	16.2±2.1	24.2±5.1
112D-12	40.7±8.4	61.6±1.6	26.0±2.6	34.9±12.2	28.5±3.8	26.8±5.7	37.2±2.1	22.4±3.8	19.6±3.4	21.9±4.5
112D-18	38.1±2.7	62.5±10.3	27.1±11.4	33.3±6.3	21.5±4.1	16.3±4.3	28.9±3.9	22.1±3.0	13.4±2.5	16.1±1.2
112D-19	41.4±9.5	52.9±10.7	22.5±9.7	31.2±11.5	13.8±3.9	28.7±13.0	31.7±3.0	31.9±6.3	14.0±1.9	9.5±0.3
BG1-9	35.3±3.0	16.2±4.6	74.5±14.0	27.0±3.4	23.4±2.1	31.7±6.4	38.6±4.4	14.3±4.2	16.2±1.0	35.7±1.9
BG1-10	33.7±1.0	20.9±1.9	72.8±15.4	49.7±3.5	16.3±2.6	23.0±5.4	27.9±5.1	25.2±5.3	9.5±1.1	28.5±0.8
IGR-4	37.5±12.0	22.4±12.5	24.9±9.4	53.0±6.9	15.9±4.2	30.7±6.5	11.3±3.1	22.1±6.7	25.2±8.1	26.1±1.1
IGR-5	51.3±10.5	20.0±11.0	52.1±10.4	51.8±3.8	9.2±3.1	33.5±13.9	16.2±2.1	15.7±1.9	33.7±2.9	23.3±4.3
IGR-15	41.6±9.0	18.5±6.2	26.8±4.5	27.1±4.3	13.2±4.5	38.1±7.8	18.9±3.4	16.1±4.4	28.0±5.1	11.9±3.2

VIII. Student's *t*-test analysis of OvCa-specific aptamers for the capture rates of multiple cancer cell lines

We applied a statistical method, the Student's *t*-test, to analyze the statistical data listed in Supplemental Table 2. These statistical results are listed in Supplemental Table 3. The capture rate of the aptamer, 112D-9, toward the target cell, TOV112D, was 58.8±8.3%; while it was 39.9±11.6% for TOV21G, 28.3±9.5% for BG1, 30.1±5.5% for IGROV1, 29.1±2.9% for MCF7, and 34.1±0.8% for A549. When compared with the capture rate of TOV112D, the capture rate of TOV21G shows a significant difference from that of TOV112D (p value=0.010＜0.050). Similarly, the capture rate of BG-1 shows a significant difference from that of TOV112D (p value=0.001＜0.050). Again, the capture rate of IGROV1 shows a significant difference from

TOV112D (p value=0.003＜0.050). When compared with the capture rate of TOV112D, the capture rate of MCF7 shows a significant difference from that of TOV112D (*p* value=0.011＜0.050). Similarly, when compared with the capture rate of TOV112D, the capture rate of A549 shows a significant difference from TOV112D (*p* value=0.029＜0.050).

Furthermore, the capture rate of aptamer, 112D-12, to the target cell, TOV112D, was 61.6±1.6% while it was 40.7±8.4% for TOV21G, 26.0±2.6% for BG1, 34.9±12.2% for IGROV1, 28.5±3.8% for HeLa, 26.8±5.7% for MCF7, and 37.2±2.1% for A549. When compared with the capture rate of TOV112D, the capture rate of TOV21G shows a significant difference from that of TOV112D (*p* value=0.033＜0.05). Similarly, when compared with the capture rate of TOV112D, the capture rate of BG-1 shows a significant difference from that of TOV112D (*p* value=0.001＜0.050). Again, the capture rate of IGROV1 shows a significant difference from that of TOV112D (*p* value=0.006＜0.050). Furthermore, when compared with the capture rate of TOV112D, the capture rate of HeLa shows a significant difference from that of TOV112D (*p* value=0.001＜0.050). Again, the capture rate of MCF7 shows a significant difference from TOV112D (*p* value=0.004＜0.050). The capture rate of A549 also shows a significant difference from that of TOV112D (*p* value=0.001＜0.050).

The capture of the aptamer 112D-18 to the target cell TOV112D was 62.5±10.3% while it was 38.1±2.7.% for TOV21G, 27.1±11.4% for BG1, 33.3±6.3% for IGROV1, and 28.9±3.9% for A549. The capture rates of TOV21G, BG-1, IGROV1 and A549 show significant differences from that of TOV112D (p value=0.031＜0.050).

Similarly, the capture of the aptamer 112D-19 to the target cell TOV112D was 52.9±10.7% while it was 41.4±9.5% for TOV21G, 31.2±11.5% for IGROV1, 28.7±13.0% for MCF7, 31.7±3.0% A549, and 31.9±6.3% for HepG2. The capture rates of TOV21G, IGROV1, MCF7, A549, and HepG2 show significant differences from that of TOV112D (p value=0.003＜0.050).

The capture rate of the aptamer BG1-9 to the target cell BG-1 was 74.5±14.0% while it was 35.3±3.0% for TOV21G, 27.0±3.4% for IGROV1, 31.7±6.4% for MCF7 38.6±4.4% for A549, and 35.7±1.9% for NIH3T3. The capture rates of TOV21G, IGROV1, MCF7, A549, and NIH3T3 show significant differences from that of BG-1 (p value=0.025＜0.050).

The capture rate of the aptamer BG1-10 to the target cell BG-1 was 72.8±15.4% while it was 33.7±1.0% for TOV21G, 49.7±3.5% for IGROV1, 27.9±5.1% for A549, 25.2±5.3% for HepG2, and 28.5±0.8% for NIH3T3. The capture rates of TOV21G, IGROV1, A549, HepG2, and NIH3T3 show significant differences from that of BG-1 (p value=0.042＜0.050).

The capture of the aptamer IGR-4 to the target cell IGROV1 was 53.0±6.9% while it was 37.5±12.0% for TOV21G, 30.7±6.5% for MCF7, 25.2±8.1% for M2-B104, and 26.1±1.1% for NIH3T3. The capture rates of TOV21G, MCF7, M2-B104, and NIH3T3 show significant differences from that of IGROV1 (p value=0.034＜0.050).

Similarly, the capture of the aptamer IGR-5 to the target cell IGROV1 was 51.8±3.8% while it was 33.5±13.9% for MCF7, and 33.7±2.9% for M2-B104. The capture rates of MCF7 and M2-B104 show significant differences from that of IGROV1 (*p* value=0.046＜0.050).

Supplemental Table 4: Statistical analysis of the Student's *t*-test for the capture rates of the selected aptamers

Aptamer	112D-9	112D-12	112D-18	112D-19	BG1-9	BG1-10	IGR-4	IGR-5
Cell line	TOV112D				BG-1		IGROV1	
	p value							
TOV21G	0.010	0.033	0.031	0.003	0.025	0.042	0.034	-
TOV112D	-	-	-	-	-	-	-	-
BG-1	0.001	0.001	0.001	-	-	-	-	-
IGROV1	0.003	0.006	0.001	0.004	0.016	0.032	-	-
HeLa	-	0.001	-	-	-	-	-	-
MCF7	0.011	0.004	-	0.002	0.010	-	0.001	0.046
A549	0.029	0.001	0.011	0.041	0.023	0.017	-	-
HepG2	-	-	-	0.014	-	0.014	-	-
M2-B104	-	-	-	-	-	-	0.001	0.001
NIH3T3	-	-	-	-	0.031	0.005	0.015	-